Mechanical properties of ceramic filled aluminum metal matrix composites: An Experimental and Computational analysis

Deepika Shekhawat
MNIT Jaipur
Pankaj Agarwal
MNIT Jaipur
Amit Singh
MNIT Jaipur
Tej Singh
Savaria Institute of Technology, Eötvös Loránd University
Amar Patnaik (apatnaik.mech@mnit.ac.in)
MNIT Jaipur

Research Article

Keywords: Nano-zirconia, Stir casting, Finite element analysis, Mechanical properties, Representative volume element

Posted Date: July 5th, 2022

DOI: https://doi.org/10.21203/rs.3.rs-1748056/v1

Abstract

With each passing year, new research is being carried out to discover materials with enhanced load-bearing capacity for prostheses and medical equipment. This study deals with the fabrication and mechanical testing of nano-zirconium oxide (n-ZrO_2; 0–15 wt.%; at steps of 5%) reinforced Al 6061 prepared via a stir casting process. The effect of n-ZrO_2 loading on physical and mechanical properties along with the detailed characterization has been systematically investigated. The density (2.6491–2.6812 g/cc), hardness (85–103 HV), tensile strength (147–227 MPa), tensile modulus (75–99 GPa), flexural strength (312–450 MPa), and impact strength (23–45 J) improved by increasing the wt.% of n-ZrO_2 reinforcement particles. Furthermore, representative quantity element-based computational homogenization modeling was used to evaluate physical and mechanical properties. It was found to be in good agreement with the experimental results within a deviation of ~ 5%. The implication of these findings shows that 5 wt.% nano-ZrO_2 reinforced Al 6061 composites (Al-ZC1) yielded better performance than pure Al 6061 alloy. This novel and comprehensive similarity throughout the examined properties for intricate microstructures perhaps be beneficial for designing optimum composite structures for prosthetic and orthotic applications.

1. Introduction

Prosthetic devices are generally used by patients who have had an amputation. These artificial devices or prostheses usually restore the mobility and locomotion of the children, adolescents, and elderly people affected by amputation. Amputation types include above knee (thigh, knee, foot, and toes removal), below knee (lower leg, foot, toes removal), arm, hand, finger, foot, and toe amputation. These amputations are caused as a result of musculoskeletal imbalances or pathologies, accident, trauma, or illness that causes physical disorders or problems that limits person's mobility [1].

Particle (micron- and nano-sized) reinforced metal matrix composites are gaining attention these days owing to their wide applications in lightweight medical devices. Aluminium devices are easily manufactured into whatever shape is enviable, making them advantageous for medical equipment that must be made to precise specifications. The aluminium matrix composites owing to their design flexibility has contributed to the advancement of medical devices. The adaptability of aluminium alloy to engross distinguished reinforcements into it be it continuous, discontinuous, or dispersed particulates makes them the most acceptable and suitable material for exploring its implementation in different biomedical applications [2–4] Distinguished metallurgical routes are adopted to fabricate such particle reinforced composites, namely stir casting, friction stir processing, spark plasma sintering, etc., of which stir casting is the most favoured approach. Liquid metallurgical mode (stir casting) is one of the best and most frequently acknowledged primary fabrication procedures for aluminium-based composites [5, 6]. Stir casting offers numerous benefits compared to other conventional procedures, including low processing costs, simple process, superior particle uniformity, mass production, minimal particle absorption, and wide range of design flexibility (shapes, sizes, and weight fraction) [7].

Past studies indicate that mechanical properties of the composites tend to improve with the incorporation of wt.% of nanoparticles in the matrix [8, 9]. Boppana et al. [10] fabricated Al6061-Al_2O_3-graphene hybrid metal matrix composites using fluid metallurgy (i.e., stir casting) route and evaluated its microstructural and mechanical characteristics. Results indicated improvement in tensile strength and yield strength with the incorporation of graphene as compared to monolithic alloy. Besides, enhancement in mechanical properties was credited to the presence of hard Al_2O_3. About 69.10% increment in hardness was observed with 1% graphene and 15 wt.% Al_2O_3.

The composites fabricated via different techniques have been widely examined and studied by using the finite element method (FEM) for estimating their behaviour and service life. Micromechanical simulation aids in delivering deeper knowledge regarding stress and damage progression within a representative volume element (RVE) of the developed ceramic-metal composites. Chawla et al. [11] developed a 3D model of SiC particle reinforced aluminium matrix composite (AMC) and utilized the finite element method to simulate it. In contrast to the experimental results, their model delivered the nearest estimation of the mechanical characteristics and Young's modulus for 20 wt.% SiC reinforced AMC.

The reported literature uncovered that hybridization of aluminium 6061 alloys with ceramic reinforcements like zirconium oxide, titanium oxide, yttrium oxide etc., yielded enhanced mechanical performance for the biomedical devices [1, 12] The impact of reinforcing quaternary ceramics in aluminium matrix is scarcely reported. Therefore, the undertaken study is a novel study which intends to develop a series of zirconium oxide (ZrO_2), titanium oxide (TiO_2), yttrium oxide (Y_2O_3), and strontium oxide (SrO) filled Al 6061 composites (viz. Al-ZC0, Al-ZC1, Al-ZC2, and Al-ZC3) appertaining to a combination of varying zirconium oxide from 0, 5, 10, to 15 wt.%, 12 wt.% titanium oxide, 6 wt.% yttrium oxide, and 3 wt.% strontium oxide in an attempt to fabricate a durable material for medical devices. The outcomes include a substantial assessment of the mechanical performance of ceramics reinforced Al matrices to elucidate the contemporary influence of adding nano-ceramics. Also, the FE-RVE (taking orthotropic properties) and FEM analysis is executed to examine the density, hardness, and tensile properties and compared with the experimental results. The findings reported here are the outcomes of preliminary investigations of the physical and mechanical behaviour arising from a small section of the composite material developed for the biomedical application especially emphasizing on external wearable medical equipments.

2. Materials And Method

2.1. Materials and fabrication details

The slabs of base matrix Aluminium alloy (Al 6061, melting point = 650°C) is locally supplied by Savita Scientific & Plastic Products Ltd, Jaipur, Rajasthan; with confirmed elemental content by Materials Research Centre, MNIT Jaipur as tabulated in Table 1.

Table 1
Chemical composition of aluminium 6061 alloy in wt.%

Composition	Fe	Mn	Mg	Cu	Zn	Si	Cr	Ti	Al
AA6061	0.23	0.03	0.84	0.22	0.10	0.62	0.22	0.1	Balance

The other materials procured includes; Zirconium oxide (ZrO_2) (supplied by Alfa Aesar, Hyderabad, particle size ~ 25 nm, 99% pure); Yttrium (III) oxide (Y_2O_3) (supplied by Alfa Aesar, Hyderabad, particle size ~ 67 nm, 99.99% pure); Titanium (IV) oxide (TiO_2), (supplied by Alfa Aesar, Mumbai, particle size ~ 32 nm, 99.9% pure); Strontium oxide (SrO) (supplied by Sigma-Aldrich, USA, particle size, ~ 52 nm, 99.9% pure). The SEM images and particle size distribution of the used ceramics are depicted in Fig. 1a-d.

In current study, stir casting technique is adopted for fabricating the ceramic reinforced metal matrix composites. The composites with 0, 5, 10, and 15 wt.% of ZrO_2 are synthesized as tabulated in Table 2. Before casting, the procured ceramic powders, are ball milled for 3 h in a tungsten vial by utilizing tungsten grinding media with a ball: powder ratio of 10:1 at 300 rpm for homogenization. The Al 6061 ingots are melted in a muffle furnace at a temperature of 750°C, and the preheated ball milled ceramic particulates are mixed into the Al matrix so as to ease the dispersion of nanoparticles into the molten matrix [13, 14]. Further, molten Al 6061 is accompanied by stirring at a speed of 300 rpm for 10 minutes, and ceramic particulates are added through the vortex created by the stirring process in the presence of argon gas flow (to eradicate process by-products and air that is present initially in the processing compartment) [8, 15]. For enhancing the wettability between the matrix and ceramics, the magnesium powder (2 wt.%) is incorporated into the mixture to reduce the surface tension of Al matrix and maintain adequate wettability between the constituents.

Table 2
Formulation design

Designation	Elements				Base matrix
	ZrO_2 (wt.%)	Y_2O_3 (wt.%)	TiO_2 (wt.%)	SrO (wt.%)	Al 6061
Al-ZC0	0	6	12	3	Bal.
Al-ZC1	5	6	12	3	Bal.
Al-ZC2	10	6	12	3	Bal.
Al-ZC3	15	6	12	3	Bal.
*Al-ZC: Al 6061- Zirconium oxide (0, 1, 2, 3→ 0, 5, 10, 15 wt.% ZrO_2) composites					

2.2 Measurements

2.2.1 Microstructural characterization

The samples from ZrO_2-free and ZrO_2-containing fabricated composites are tested to determine reinforcement dispersion, microstructure, elements present, surface morphology, and interface formation process. The surface morphology of the samples is examined by using FEI NOVA NANO 450 scanning electron microscope (FE-SEM, Zeiss, SUPRA 40 VP) attached with energy-dispersive elemental (EDS) analyser operating at 15 KV. An X'Pert3 powder diffractometer (PANalytical, Netherland) is utilized to acquire the XRD (X-ray diffraction) patterns, which were performed for the 2θ range of 20–80°.

2.2.2 Physical and mechanical characterization

The density and void percentage in any novel fabricated material decide its resultant mechanical performance. The numerically simulated density is evaluated using FE-RVE software, and experimental density is evaluated using Radwag AS 220.R2 equipment following standard water displacement method as per ASTM D792. Theoretical density is determined using the rule of mixture, while the normalization of the theoretical density with experimental density is used for the estimation of the void content of the fabricated composites. The Vickers hardness (NEXUS 4303 series, Europe) of the fabricated composites is evaluated by averaging the eight readings on a sample's mirror-polished surface as per ASTM E 18 standard. The tensile tests of the composites were performed on a universal testing machine (Servo-hydraulic machine, HEICO, New Delhi, India) in accordance to the ASTM E-8 standard on 90 × 15 × 4 mm^3 sized samples with 1 mm/min cross-head speed. The flexural test of the specimens is conducted on the same machine as per ASTM E290 at 1 mm/min cross-head speed. The dimension of the sample is 60 × 10 × 10 mm^3. The impact test is conducted on the samples prepared as per IS: 1598–1977 standards on a digital impact tester machine (AMT-8D, Banbros Engineering Pvt. Ltd.). Izod tests are carried out on the single-notch square test specimens of dimension 75 × 10 × 10 mm^3. For the evaluated properties, the final value is evaluated as the average of three tests.

2.3 Finite-element analysis

2.3.1 Representative volume element

The representative volume element (RVE) approach and periodic boundary condition (PBC) is adopted to comprehend properties, namely, density, elastic, and shear modulus, by utilizing the three-dimensional (3D) finite element method (FEM) simulation as shown in Fig. 2a-d.

The comprehension of the relationship between the microscopic and microstructural behaviour has been accomplished by practicing micromechanical models that take into account the matrix and reinforcing particles' properties along with their volume fractions. So, for examining the impact of particle volume fractions upon the mechanical characteristics of the ceramic reinforced metal composites finite element method has been used. The 3D model of the sample is modelled in the material designer tool of ANSYS software is, illustrated in Fig. 2e-g.

2.3.2 Finite element modelling (FEM)

The ANSYS 2020 R2 version software is employed for conducting the 3D numerical study on the composite's geometry prepared using a design modeller. This drafted geometry is further imported into FEM's sophisticated meshing tool. Meshing is generally utilized to discretize the body into nodes and elements for the refinement that aids in determining the exactitude of the solution. Therefore, program-controlled mesh with a mesh size of 0.05 mm is employed, and the geometrical and meshed isometric model of hardness test coupons are prepared. Figure 2e shows the flexural test specimen by considering all the boundary conditions related to the real-time experiments. For the hardness test, the boundary conditions are the input load given to the modelled diamond indenter as shown in Fig. 2e and fixed support at the bottom of the test specimen. These are implemented to the meshed body in the analysis settings of the explicit unit of the FEA package. In this numerical analysis, the base Al 6061 matrix is assumed to be an elastoplastic material (inclusive of damage) and the ductile damage model is utilized for predicting the damage evolution owing to nucleation, development, and fusion of cavities.

3. Results And Discussion

3.1 Microstructural characterization

The microstructure images and corresponding EDAX pattern of the manufactured composites with different ZrO_2 content are presented in Fig. 3a-d. With increasing ZrO_2 content, flaky type features were identified along with few pores/voids are also presented in the composites. EDAX analysis for Al-ZC0 (Fig. 3a) detected by SEM confirms the presence of Al, Ti, Y, Sr, and O elements throughout the composite, indicating the presence of TiO_2, Y_2O_3, and SrO particulates, whereas no peaks were observed for Zr element indicating the absence of ZrO_2 particles in the aluminium matrix.

Whereas the EDAX results for other composites (Fig. 3b-d) indicate the presence of all the reinforced elements, i.e., Al, Zr, Ti, Sr, Y, and O in the Al 6061 matrix, confirming the presence of ZrO_2, TiO_2, Y_2O_3, and SrO. Besides, the EDAX mapping results are also reported for Al-ZC0 (Fig. 4a) and Al-ZC3 (Fig. 4b) composites. The elemental mapping also revealed that all the stated elements are adequately dispersed inside the composite. The distracted provinces in the elemental mapping images are represented by the black regions due to the surface irregularities, so no element was recognized in these regions [16].

3.2 XRD analysis

X-ray diffraction characterization is a useful method for determining the characteristics of the fabricated composites made up of different ceramic powder mix constituents such as ZrO_2, TiO_2, Y_2O_3, and SrO. Each XRD pattern depicts the generated phases in the samples with different percentage compositions of reinforcing filler particulates. Figure 5 depicts the obtained patterns for different compositions of ZrO_2

reinforced Al 6061 composites. The reaction compounds developed during the fabrication of the composites are detected by using XRD analysis. The peaks in the XRD plot represent the major elements present in the Al 6061 composites. Also, the peaks that are formed due to the addition of the ceramic phase, viz. ZrO_2, TiO_2, SrO, and Y_2O_3 reinforcement are also observed, and ZrO_2 peaks began to rise with the addition of a larger weight percentage of ZrO_2 in the Al 6061 matrix. For ZrO_2-containing samples, the XRD pattern depicts strong diffraction peaks of Al, Zr. The minor phases present are TiO_2, SrO, and Y_2O_3. These peaks indicate that all the reinforcing ceramic reinforcements are evenly dispersed in the Al 6061 matrix.

The peak position of ZrO_2 is observed, with some approximate equivalent 2θ values of 25.075° (JCPDS 00-017-0385 data file) and 41.305° (JCPDS 00-013-0307 data file), and at these peaks, the intensity of ZrO_2 is greater. Whereas for others, the peaks with the 2θ values of 38.515° (JCPDS 00-004-0787 data file) and 45.545° (JCPDS 01-071-3760 data file) are observed for Al, 65.125° (JCPDS 00-015-0875 data file) is observed for TiO_2, 82.435° (JCPDS 00-043-0661 data file) is observed for Y_2O_3, 78.205° (JCPDS 00-015-0288 data file) is observed for SrO. The ZrO_2 particle diffraction peaks are clearly visible, and the intensity of the peaks tends to increase with the increased percentage of ZrO_2. In the fabricated composites, no peak attributed to an undesirable intermetallic phase formed is observed. This is because, during the casting process in the temperature range of 655°C to 750°C, no chemical reactions occur that can cause new phases to form between the ZrO_2, TiO_2, Y_2O_3, and SrO particles, and the Al 6061 matrix at such a low temperature [17].

3.3 Density and void content

The experimental density (2.6491–2.6812 g/cc), theoretical density (2.6593—2.6812 g/cc), and FE-RVE density of the fabricated composites are presented in Table 3, which indicates that density increases progressively owing to the higher density of the reinforcing phase, i.e., zirconia (density = 5.89 g/cc) whose proportion is enhanced by 5% step across the formulation and other fixed composition ceramics TiO_2, Y_2O_3, and SrO. A similar trend was observed by Hemanth and Divya [22] while fabricating nano-ZrO_2 (100—200 nm) in wt.% of 3 to 15 (steps @ 3 wt.%) and Pul [23] while fabricating ZrO_2 in wt. % of 5 to 20 (steps @ 5 wt.%) reinforced aluminium alloy composites. From Table 3, it can be clearly noted that the experimental density of the composites is less as compared to the theoretical values. The obtained density values align with the density values required for load bearing central pylon components.

Table 3
Density and void content of the composites

Composite	Density (g/cc)			Void content (%)	Experimental and FE-RVE error (%)
	Theoretical	Experimental	FE-RVE		
Al-ZC0	2.6593	2.6491	2.6553	0.38	4.97
Al-ZC1	2.6743	2.6618	2.6721	0.46	2.93
Al-ZC2	2.6895	2.6724	2.6852	0.63	4.00
Al-ZC3	2.7057	2.6812	2.6947	0.90	3.89

This is attributed to the fact that theoretical density is evaluated considering the ideal perfect state within the material, which differs, in reality, owing to inadequacies. The density evaluated using FE-RVE model (Table 3) indicates that the measured density is lower than the numerically simulated results, which can be attributed to the presence of porosity. The variance in the ideal perfect state derogates the density by encouraging the inception of porosity or voids in the composites, and these may be estimated in the context of void content/percentage. The void fraction (~ 0.38–0.90%; Table 3) demonstrates an increasing trend with the rising percentage of the harder phase, indicating that the presence of ZrO_2 in the Al 6061 matrix facilitates the interfacial bonding between the constituent elements and fine microstructure, similar results were reported by Ezatpour et al. [19] The prime reason may be the adopted fabrication (stir casting) technique for this minor increase in void content which may not be observed when prepared with other advanced fabrication routes like spark plasma sintering, hot press sintering, etc. [9]. Secondly, the presence of other ceramic particulates (TiO_2, Y_2O_3, SrO) in the matrix may be accountable for this increase. This is how the occurrence of a modest amount of porosity can be explained. When compared to molten aluminium, the semisolid slurry absorbs less gas. When the semisolid slurry is sent to the mould, a significant amount of it solidifies. Solidification shrinkage-related porosities are unlikely to occur. These voids or porosities are contributing reason for the generation of stress concentration which procreates multi-crack initiation-propagation in the material, causing materials to fail early or fracture during the actual functioning [5].

3.4 Mechanical properties

3.4.1 Hardness

The impact of varying the wt.% of ZrO_2 particles on the hardness values can be perceived in Fig. 6. For every weight fraction of ZrO_2 (0, 5, 10, and 15 wt.%), the fabricated ceramic-metal composites demonstrated hardness viz. 85 HV, 94 HV, 97 HV, and 103 HV for Al-ZC0, Al-ZC1, Al-ZC2, and Al-ZC3 respectively. In composites reinforced with ZrO_2, TiO_2, Y_2O_3, and SrO, the hardness values demonstrated an increase in parallel with the increase in ZrO_2 weight percentage by forming a strain in the matrix structure [20] When the percentage of ZrO_2 (harder phase) increases, the reinforcement-to-matrix ratio gets richer in ZrO_2, enhancing the composite's hardness and material's resistance to plastic deformation.

The size of the reinforcement and the wt.% of reinforcement were the two most important factors influencing the hardness of the stir-cast composites [21] Reinforcing ceramic nanoparticles increases the hardness owing to grain refinement, the Hall–Petch process, and particle strengthening effects [19] Al-ZC3 composite showed the highest hardness as a result of grain refinement and reduction in dislocation density. This impact was brought about as a result of the high porosity content and the heterogeneous dispersion of nanoparticles [24].

The hardness of the developed composites was further evaluated by the use of the finite element method by modelling the test specimens and pyramidal diamond indenter in the Ansys Design modeller using explicit dynamics. The numerically simulated results are then compared with experimental values, and the difference is shown in percentage error in Fig. 6a. The primary objective to carry out this numerical simulation is to visualize the displacement of the indenter by the application of force exerted and imprint of indenter on the surface of test coupons. The crater created by the indentation is seen in Fig. 6b, and the depth of the crater is evaluated. The numerical values evaluated after the simulations are presented in the form of equivalent von mises stresses, as shown in Fig. 6c-f. The penetration depth as a function of hardness is found to decrease with respect to the increasing weight percentage of nano-zirconia particulates in the Al 6061 matrix.

3.4.2 Tensile properties and its morphological study

The tensile strength and tensile modulus of the ceramic reinforced metal matrix composites are presented in Fig. 7(a). A linear increment can be observed in the tensile properties with increasing n-ZrO_2 loading, reaching a relative improvement of ~ 54% for tensile strength and 32% for tensile modulus with 15 wt.% of n-ZrO_2 content. The increased tensile strength values are the result of resistance to dislocation movements, density, and their interaction with the reinforcing ceramic particulates. By the strengthening mechanism, ZrO_2 particles communicate their strength to the matrix alloy; the load on the matrix is shifted to the reinforcing particles, resulting in composites that are more resistant to produced tensile stress. The reinforcement of ceramic particulates (ZrO_2) into the matrix of Al 6061 affected the micromechanics of the matrix.

It can be clearly observed that when particle support is brought into the molten matrix of Al 6061 alloy, owing to a significant difference in their thermal expansion coefficient, there is a huge escalation in the dislocation density throughout the composite. This increment in the tensile strength may be ascribed due to the diminished grain size of the matrix material and the enhancement in the dispersion of ceramic particulates [24, 25]. For Al-ZC0 composite, the tensile modulus is 75.06 GPa, and with an addition of 5 wt.% n-ZrO_2 content, 15% increase in tensile modulus is observed. For the composite with 15 wt.% n-ZrO_2 content (i.e., Al-ZC3), the tensile modulus remains highest with a value of 99.21 GPa, exhibiting an improvement of ~ 32%. Moreover, the formation of rigid interfaces within the soft matrix in the presence of small-sized ceramic fillers (n-ZrO_2 in this case) of higher stiffness can also be ascribed to the decreased tensile modulus of the composites. The fractured samples were examined to understand the failure/fracture mechanism using SEM and depicted in Fig. 8.

As can be observed, the fractured surfaces of Al-ZC0 revealed some deep equiaxed dimples as shown in Fig. 8a, demonstrating the phenomenon of substantial plastic deformation just prior to actual failure. As a result, the composite fracture is anticipated to be ductile due to the construction and fusion of micro-voids. During the tensile process, certain cleavage fractures and fracture bands were noticed in SEM micrographs of Al-ZC0. It can be claimed that during tensile testing, micro-voids occur under a local three-dimensional condition of stress and proliferate as the tensile load increases. Finally, the voids grow to a critical size, and the micro-voids merge, causing a fracture.

The fractured surfaces of Al-ZC1 indicated the presence of deep dimples signifying higher plastic deformation prior to fracture and cleavage facets in some areas, as shown in Fig. 8b. The fractured surface of Al-ZC2 (Fig. 8c) reveals the presence of shallower dimples as compared to Al-ZC0 and Al-ZC1 composites, pointing to a lower plastic deformation before fracture. Hence, the fracture surfaces of ceramic reinforced aluminium matrix composites exhibit the ductile behaviour of the Al 6061 matrix. The fracture images of Al-ZC3 (Fig. 8d) revealed minute-sized dimples and some cleavage features due to stress concentration in these areas, pointing out the formation of cracks at the ceramic particles and aluminium matrix interface then these cracks propagate, thereby indicating failure owing to brittle fracture. It is concluded that increasing the weight fraction of n-ZrO_2 reinforcing particulates reduces the composites' ductility.

Further, the finite element simulation is executed to numerically prognosticate the tensile behaviour of the ceramic reinforced Al-6061 matrix composites as presented in Fig. 9c-f. The numerically simulated values are compared with the experimental results depicted in Fig. 9a,b and it can be observed that both the values are in great harmony. This demonstrates that the finite element model and material model employed while simulating is infallible in anticipating the tensile behaviour of ceramic reinforced aluminium 6061 matrix composite specimens. The obtained tensile results align with the tensile values attained by Kadhim et al. [25] who compared the materials for lower limb prosthesis.

3.4.3 Flexural strength

The flexural strength of n-ZrO_2 filled composites is shown in Fig. 10a,b and showed an increasing trend with increased filler loading. The flexural strength of the manufactured composites was increased by ~ 14% from 312 MPa (Al-ZC0) to 356 MPa (Al-ZC1) for 5 wt.% n-ZrO_2 filled composites. As the content of n-ZrO_2 reinforcement increased to 15 wt.%, an improvement of ~ 42% was noted for composite Al-ZC1 with the highest value of flexural strength of 450 MPa. The addition of n-ZrO_2 to the Al 6061 matrix raises the bending stress and forms the deformation fields. During solidification, the reinforcements function as a heterogeneous catalyst in the Al matrix. The soft particles function as lubricants and boost interfacial bonding strength, increasing flexural strength. It can be observed that reinforcing ceramic particulates improves the flexural strength of the composites as these nano-particulates function as a crack barrier wherever the cracks originated at the debonded particle/matrix boundary.

The superior bonding attributes of the matrix/particle interface imparted the enhanced flexural strength values. Along with this, the fine and nano-sized ceramics plays crucial role in enhancing the surface area and bestows improved strength in the fabricated composites. The flexural study indicates that the presence of zirconia particles in the alloy matrix has a pronounced influence as these hard and brittle zirconia particles lead to superior dislocation density inside the metal matrix. Similar results were obtained by Pazhouhanfar and Eghbali [27]. Further, finite element simulation is executed to numerically prognosticate the flexural behaviour of the manufactured composites and compared with the experimental values as presented in Fig. 10a. The deviation of FEA simulation from experimental results is ~ 1.77% for Al-ZC0, ~ 4.71% for Al-ZC1, ~ 1.26% for Al-ZC2, and ~ 3.59% for Al-ZC3. The flexural strength values attained from the simulation are in close agreement with the values obtained from standard experimental testing with an error percentage of ~ 1 to 5%. The proposed FEM analysis validates results for the structural strength of the intrinsic components (pylon tube) of the prosthetics [28].

Figure 10c-f attests the FEM simulation images for the flexural tests of the ceramic reinforced Al 6061 composites viz. Al-ZC0, Al-ZC1, Al-ZC2, and Al-ZC3 dispensing the stress plots. It can be clearly observed from the images that Al-ZC3 represents the maximum equivalent (Von-Mises) stresses of 453.04 MPa compared to experimental values within 3.46 percentage of error. The reinforcing ceramic particulates improve the flexural strength of the composites as these nano-particulates function as a crack barrier wherever the cracks originated at the debonded particle/matrix boundary. The superior bonding attributes of the matrix/particle interface imparted the enhanced flexural strength values [8]. Along with this, the fine and nano-sized ceramics plays crucial role in enhancing the surface area and bestows improved strength in the fabricated composites. The flexural strength values attained from the ANSYS are in close agreement with the values obtained from standard experimental testing. The outcomes of the finite element simulation endorse the geometrical conditions.

3.4.4 Impact energy

The impact energy exhibited a steady improvement with increasing ZrO_2 content reaching a relative increment of ~ 95% for the composite Al-ZC3 (45 J) compared to that of Al-ZC0 (23 J), as shown in Fig. 7b.

The stronger interfacial adhesion between reinforcement and matrix effectually enhances the impact-load bearing competency. The fracture in particulate-filled composites is connected with particle fracture, interfacial-matrix failure, and inclusion fracture, relying on the desired composite and the matrix condition. The regions with a large volume fraction of particulates indicate the presence of preferential void nucleation, indicating the importance of local plastic constraints [29]. The morphology of the fractured surfaces of manufactured composites was further analysed using SEM and depicted in Fig. 11.

The SEM fractographs of Al-ZC0 (Fig. 16a) impact specimens reveal that un-reinforced matrix alloy showed larger dimples along with the voids as compared to in-situ composite systems, thereby indicating the ductile fracture mode. In contrast, the micrograph of the fractured Al-ZC1 (Fig. 16b) sample shows the presence of fatigue striations, cleavage facet, and micro-voids. Similarly, Al-ZC2 (Fig. 16c) and Al-ZC3 (Fig. 16d) SEM micrographs revealed the presence of small and shallow dimples, tear ridges, voids, secondary crack, fatigue striations, and cleavage facets contributing to brittle fracture. All these reasons contribute to lesser ductility as compared to the matrix Al 6061. This indicates that composite behaviour and fracture are monitored by matrix condition [25]. Al 6061 composites with ceramic reinforcements possess greater physical and mechanical characteristics, making them a potential material for prosthetic devices with optimized strength [30, 31]

4. Conclusions

In the current study, the physical and mechanical behaviour of the fabricated ceramic reinforced Al 6061 matrix composites is investigated by varying the nano zirconium oxide (n-ZrO_2) particulates in the range 0–15 wt.% (along with the fixed wt.% of TiO_2, Y_2O_3, and SrO) by fabricating using the stir casting technique. The investigation of ceramic reinforced aluminium matrix composites displayed the following results;

- The experimental density (2.6491–2.6812 g/cc) and theoretical density (2.6593–2.7057 g/cc) of the composites increase progressively owing to the higher density of the reinforcing phase. The hardness of the composites increased with the weight percentage of nano-zirconia (85–103 HV), owing to the harder ceramic particles in the matrix.
- The tensile strength of the fabricated composites (Al-ZC0, Al-ZC1, Al-ZC2, and Al-ZC3) increased (137.73–186.1 MPa) with the increase in the weight percentage of nano-zirconia that is attributed to the resistance to dislocation movements, density and their interaction with the reinforcing ceramic particulates. Whereas Young's modulus of composites determined by the slope of the stress-strain curve within the elastic limit decreased (12.98–8.50 GPa). The stronger interfacial adhesion between reinforcement and matrix effectually enhances the impact strength (23–45 J) of the fabricated composites. The SEM observation of the fractured surfaces revealed the presence of dimples which indicates that ductile rupture is the predominant failure mechanism.
- The bending strength of the fabricated composites conducted in three-point bending mode increases with the increase in the weight percentage of the nano zirconia (312–450 MPa). The presence of zirconia particles in the matrix has a pronounced influence due to their hardness and brittleness that leads to the superior dislocation density inside the metal matrix.
- FE-RVE and FEM results obtained are in good agreement with the experimental values within a deviation of ~ 5% (error).

The porosity affects the quality and reliability of the casted composites in real-life implementation; thus, removal or minimization of these unfavourable effects is vitally important. Also, these porosities are contributing reason for the generation of stress concentration which procreates multi-crack initiation-propagation in the material causing materials to fail early or fracture during the actual functioning. Therefore, in current study, 5 wt.% nano-ZrO_2 reinforced Al 6061 composites (Al-ZC1) yielded better performance in comparison to pure Al 6061 alloy in terms of stability, and cost efficacy. The use of ceramic reinforced-aluminium MMCs in biomedical applications that need lightweight and bio-compatible materials is a grey area for future study.

Declarations

Funding No funding was received for conducting this study.

Acknowledgments

The authors would like to acknowledge the Advanced Research Lab for Tribology and Materials Research Center (MRC), Malaviya National Institute of Technology Jaipur, India, to provide necessary fabrication and testing facilities. The first author gratefully acknowledges the Minister of Human Resource Development (MHRD) for the fellowship during her PhD work.

Author Contribution

Deepika Shekhawat has performed experiments, results analysis and prepared the write up for manuscript, Pankaj Agarwal has carried out the conceptualization and methodology of the entire manuscript, Tej Singh contributed in methodology, technical improvement and formal analysis of the manuscript, Amit Singh involved in supervision, Amar Patnaik took part in validation, supervision and visualization of the manuscript.

Conflict of Interest The authors declare that they have no conflict of interest.

References

1. Yaramenko DA, Sytenko AN, Bazhina EN (1987) Prosthetic sockets of polymerized metal:Materials, design, technology. Prosthet Orthot Int 11:135–136. DOI: https://doi.org/10.3109/03093648709078196
2. Composite Materials Handbook: Metal Matrix Composites. 2002.
3. Jayalakshmi S, and Gupta M (2015) Metallic Amorphous Alloy Reinforcements in Light Metal Matrices. (2015). DOI: https://doi.org/10.1007/978-3-319-15016-1
4. McWilliams BA, Ramesh KT, Yen CF (2013) Probabilistic response of heterogeneous particle reinforced metal matrix composites with particle size dependent strengthening. Comput Mater Sci 79:15–24. DOI: https://doi.org/10.1016/j.commatsci.2013.05.047
5. Hashim J, Looney L, Hashmi MSJ (1999) Metal matrix composites: production by the stir casting method. J Mater Process Technol 92–93: 1–7. DOI: https://doi.org/10.1016/S0924-0136(99)00118-

1

6. Aherwar A, Singh A, Patnaik A (2018) A study on mechanical behavior and wear performance of a metal – metal Co–30Cr biomedical alloy with different molybdenum addition and optimized using Taguchi experimental design. J Brazilian Soc Mech Sci Eng 7: 1–19.DOI: https://doi.org/10.1007/s40430-018-1107-7
7. Chandla NK, Kant S, Goud MM (2021) Mechanical, tribological and microstructural characterization of stir cast Al-6061 metal/matrix composites—a comprehensive review. Sadhana - Acad Proc Eng Sci 46(1): 1-38. DOI: https://doi.org/10.1007/s12046-021-01567-7.
8. Bhaskar S, Kumar M, Patnaik A (2020) Silicon Carbide Ceramic Particulate Reinforced AA2024 Alloy Composite - Part I: Evaluation of Mechanical and Sliding Tribology Performance. Silicon 12: 843–865. DOI: https://doi.org/10.1007/s12633-019-00181-x
9. Shekhawat D, Singh A, Banerjee MK (2021) Bioceramic composites for orthopaedic applications: A comprehensive review of mechanical, biological, and microstructural properties. Ceram Int 47(3):3013-3030. DOI: https://doi.org/10.1016/j.ceramint.2020.09.214
10. Boppana SB, Dayanand S, Murthy BV (2021) Development and mechanical characterisation of Al6061-Al_2O_3-Graphene hybrid metal matrix composites. J Compos Sci 5:1–15. DOI: https://doi.org/10.3390/jcs5060155
11. Chawla N, Ganesh VV, Wunsch B (2004) Three-dimensional (3D) microstructure visualization and finite element modeling of the mechanical behavior of SiC particle reinforced aluminum composites. Scr Mater 51: 161–165. DOI: https://doi.org/10.1016/j.scriptamat.2004.03.043
12. Kapti AO, Yucenur MS (2006) Mechanism and Machine Theory Design and control of an active artificial knee joint. Mech Mach Theory 41: 1477–1485. DOI: https://doi.org/10.1016/j.mechmachtheory.2006.01.017
13. Velmurugan TA, Vijay P, Murugesan A (2022) Influence of Nanoparticles Reinforcements on Aluminium 6061 Alloys Fabricated via Novel Ultrasonic Aided Rheo - Squeeze Casting Method. *Met Mater Int* 28,145-154. DOI: 10.1007/s12540-021-01036-0.
14. Das DK, Mishra PC, Singh S (2014) Fabrication and heat treatment of ceramic-reinforced aluminium matrix composites- A review. Int J Mech Mater Eng 9: 1–15. DOI: https://doi.org/10.1186/s40712-014-0006-7
15. Pauzon C, Hryha E, Forêt P (2019) Effect of argon and nitrogen atmospheres on the properties of stainless steel 316 L parts produced by laser-powder bed fusion. Mater Des 179: 107873. DOI: https://doi.org/10.1016/j.matdes.2019.107873
16. Bhaskar S, Kumar M, Patnaik A (2022) Effect of Si3N4 Ceramic Particulates on Mechanical, Thermal, Thermo-Mechanical and Sliding Wear Performance of AA2024 Alloy Composites. Silicon 14: 239-262. DOI: 10.1007/s12633-020-00810-w.
17. Khalili V, Heidarzadeh A, Moslemi S (2020) Production of Al6061 matrix composites with ZrO_2 ceramic reinforcement using a low-cost stir casting technique: Microstructure, mechanical properties,

and electrochemical behavior. J Mater Res Technol 9: 15072–15086. DOI: https://doi.org/10.1016/j.jmrt.2020.10.095

18. Mohanty RK, Mohanty RC, Sabut SK (2020) A systematic review on design technology and application of polycentric prosthetic knee in amputee rehabilitation. Phys Eng Sci Med 43: 781–798. DOI: 10.1007/s13246-020-00882-3
19. Ezatpour HR, Sajjadi SA, Sabzevar MH (2014) Investigation of microstructure and mechanical properties of Al6061-nanocomposite fabricated by stir casting. Mater Des 55: 921–928. DOI: https://doi.org/10.1016/j.matdes.2013.10.060
20. Halil K, İsmail O, Sibel D (2019) Wear and mechanical properties of Al6061/SiC/B4C hybrid composites produced with powder metallurgy. J Mater Res Technol 8: 5348–5361. DOI: https://doi.org/10.1016/j.jmrt.2019.09.002
21. Deshmanya IB, Purohit GK (2012) Development of mathematical model to predict micro-hardness of Al7075/Al_2O_3 composites produced by stir-casting. J Eng Sci Technol Rev 5: 44–50. DOI: 10.25103/jestr.051.09
22. Hemanth J, Divya MR (2018) Fabrication and Corrosion Behaviour of Aluminium Alloy (LM-13) Reinforced with Nano-ZrO_2 Particulate Chilled Nano Metal Matrix Composites (CNMMCs) for Aerospace Applications, J. Mater. Sci. Chem. Eng. 06:136–150. DOI: https://doi.org/10.4236/msce.2018.67015
23. Pul M (2021) Effect of ZrO_2 quantity on mechanical properties of ZrO2-reinforced aluminum composites produced by the vacuum infiltration technique, Rev. Metal. 57: e195. DOI: https://doi.org/10.3989/revmetalm.195
24. Kareem A, Qudeiri JA, Abdudeen A (2021) A review on AA 6061 metal matrix composites produced by stir casting. Materials (Basel) 14: 1–22. DOI: https://doi.org/10.3390/ma14010175
25. Chak V, Chattopadhyay H, Dora TL (2020) A review on fabrication methods, reinforcements and mechanical properties of aluminum matrix composites. J Manuf Process 56: 1059–1074. DOI: https://doi.org/10.1016/j.jmapro.2020.05.042
26. Kadhim FM, Chiad JS, Takhakh AM (2018) Design and Manufacturing Knee Joint for Smart Transfemoral Prosthetic. IOP Conf Ser Mater Sci Eng, 454. Epub ahead of print 2018. DOI: 10.1088/1757-899X/454/1/012078.
27. Pazhouhanfar Y, Eghbali B (2018) Microstructural characterization and mechanical properties of TiB_2 reinforced Al6061 matrix composites produced using stir casting process. Mater Sci Eng A 710: 172–180. DOI: https://doi.org/10.1016/j.msea.2017.10.087
28. Mohanty RK, Mohanty RC, Sabut SK (2022) Finite element analysis and experimental validation of polycentric prosthetic knee. Mater Today Proc. DOI: 10.1016/j.matpr.2022.02.509.
29. Lloyd DJ (1991) Aspects of fracture in particulate reinforced metal matrix composites. Acta Metall Mater 39: 59–71. DOI: https://doi.org/10.1016/0956-7151(91)90328-X

30. Qadir MU, Khan MA, Hussain M (2021) Design and Analysis of Knee Joint for Transfemoral Amputees. AIMS 2021 - Int Conf Artif Intell Mechatronics 3–7. DOI: 10.1109/AIMS52415.2021.9466053
31. Anandakrishnan V, Mahamani A (2011) Investigations of flank wear, cutting force, and surface roughness in the machining of Al-6061–TiB_2 in situ metal matrix composites produced by flux-assisted synthesis. Int J Adv Manuf Technol 55: 65–73. DOI: https://doi.org/10.1007/s00170-010-3042-3

Figures

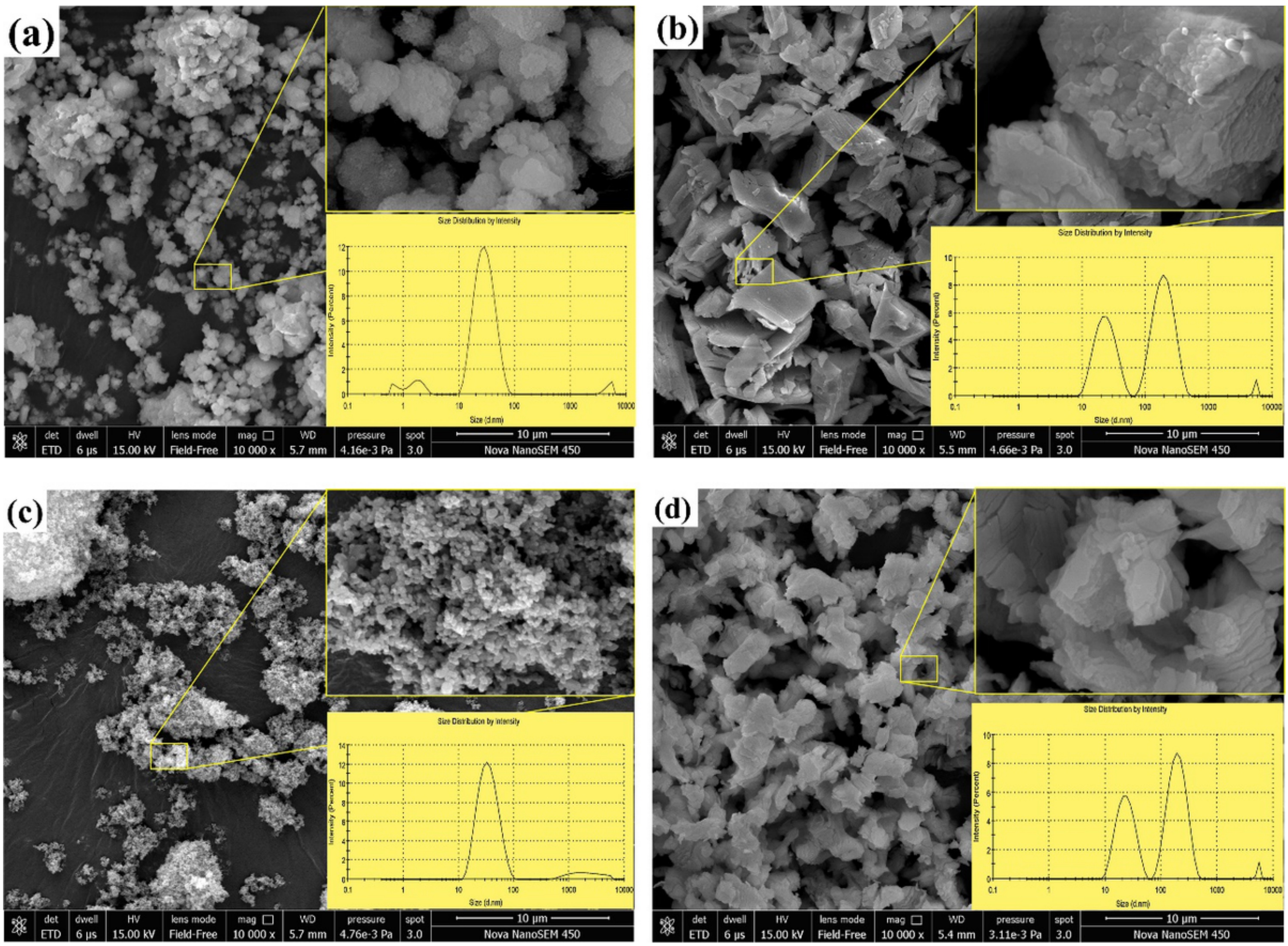

Figure 1

SEM images and size distribution of used ceramic powders (a) ZrO_2, (b) Y_2O_3, (c) TiO_2 and (d) SrO

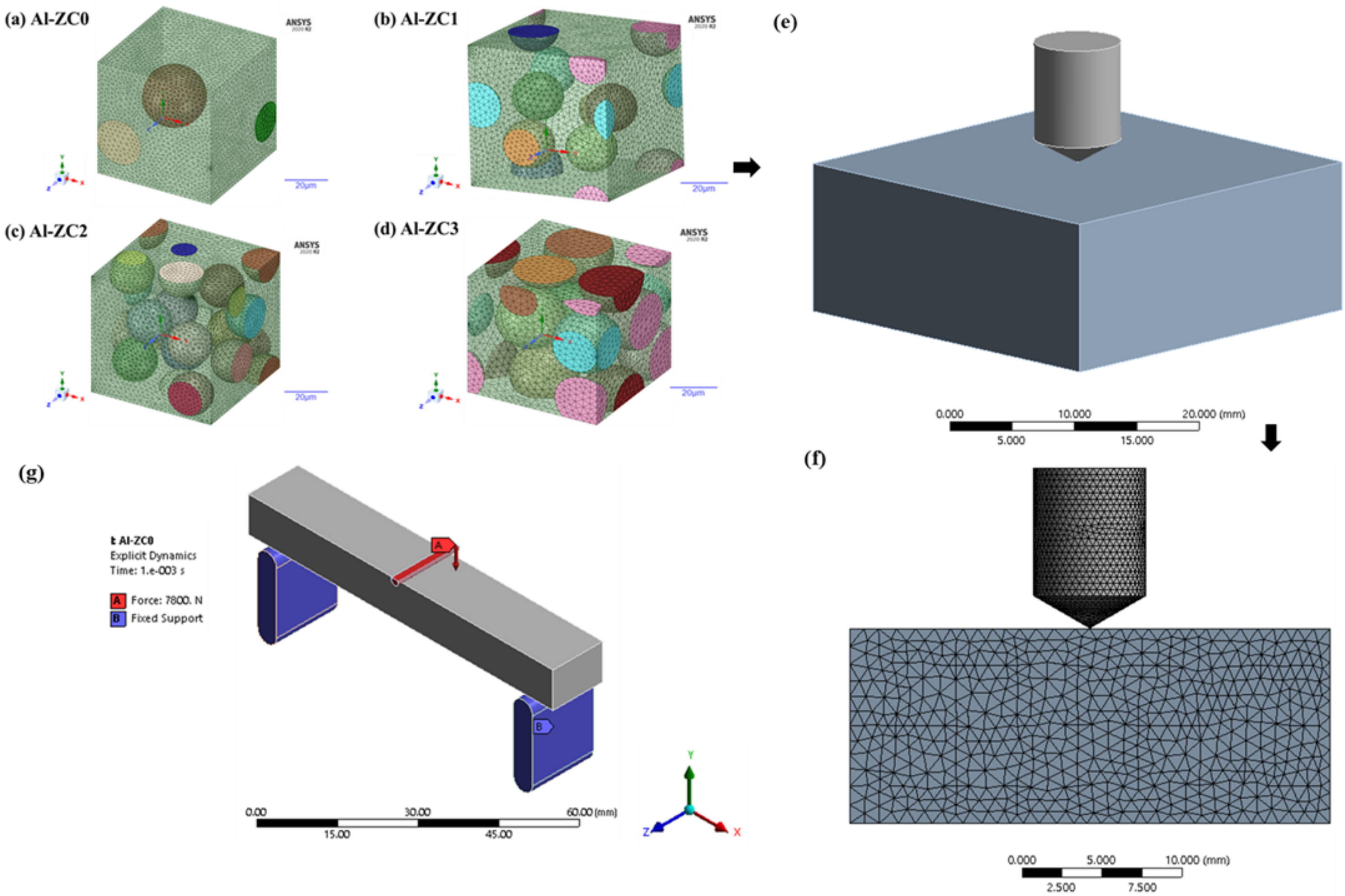

Figure 2

(a-d) Material modelling of the manufactured composites using ANSYS material designer and (e) Geometrical model, (f) Meshed isometric model of hardness sample, and (g) Flexural test sample with boundary conditions

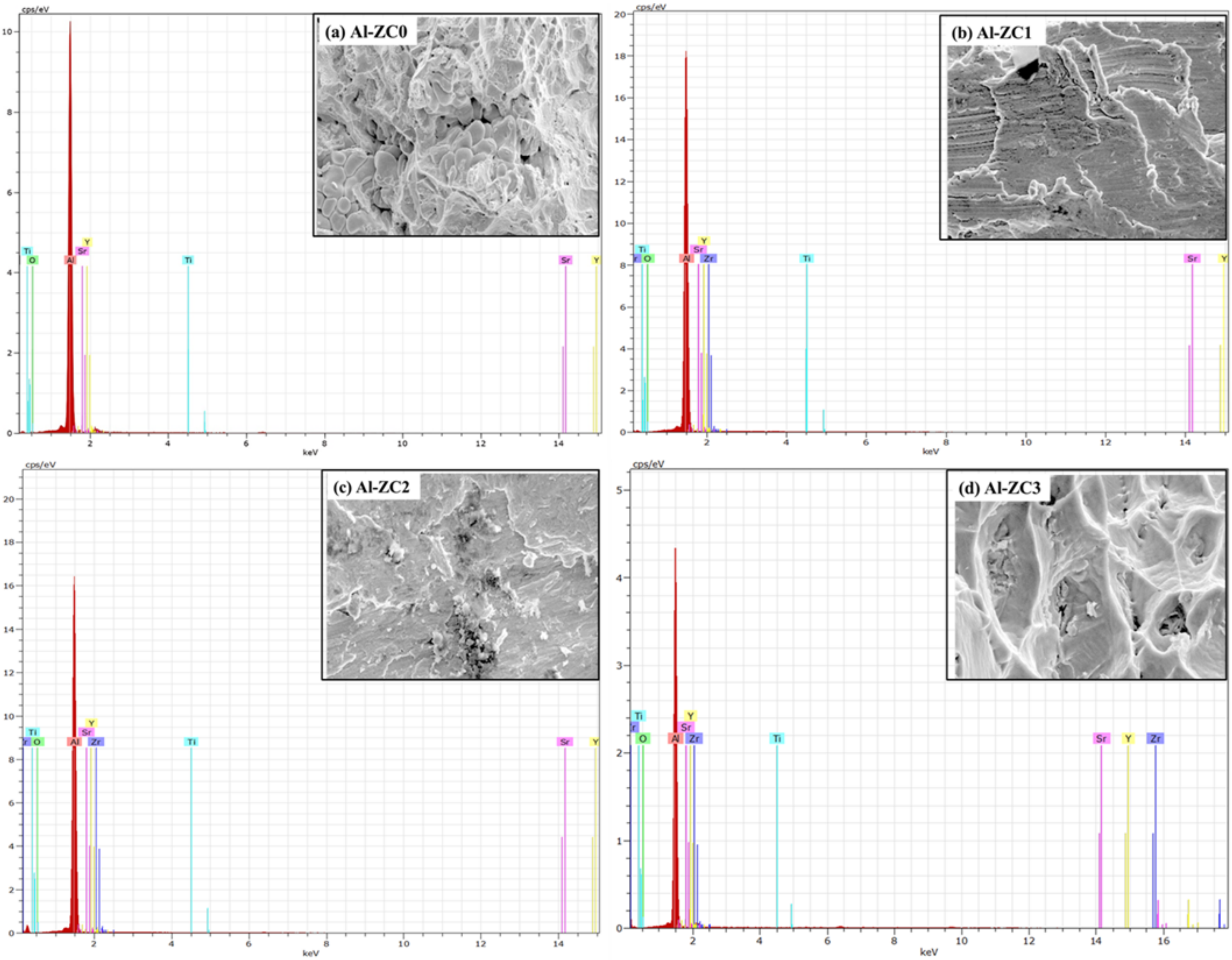

Figure 3

EDAX mapping and SEM images (inset) of the (a) Al-ZC0, (b) Al-ZC1, (c) Al-ZC2, and (d) Al-ZC3

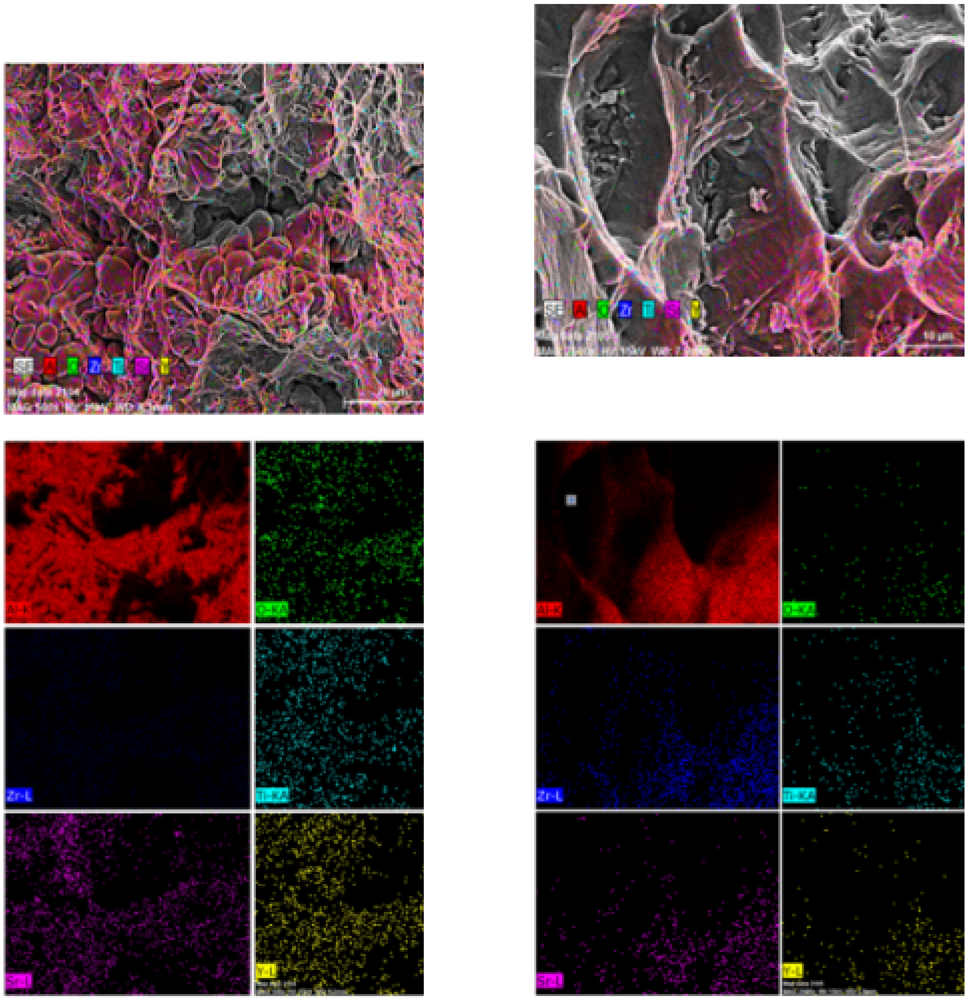

Figure 4

Elemental distribution map for (a) Al-ZC0 and (b)Al-ZC3

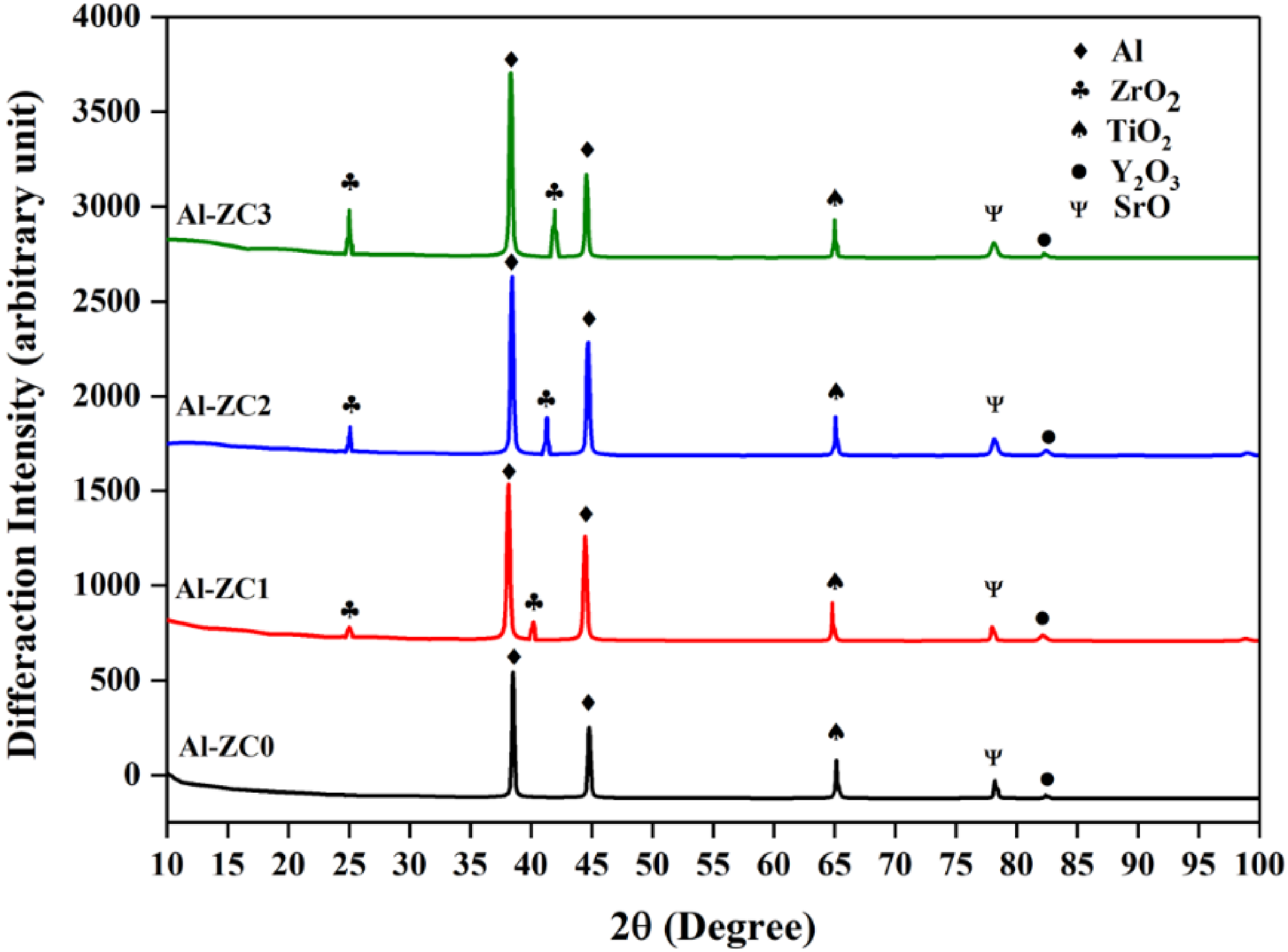

Figure 5

XRD plot of the fabricated composites

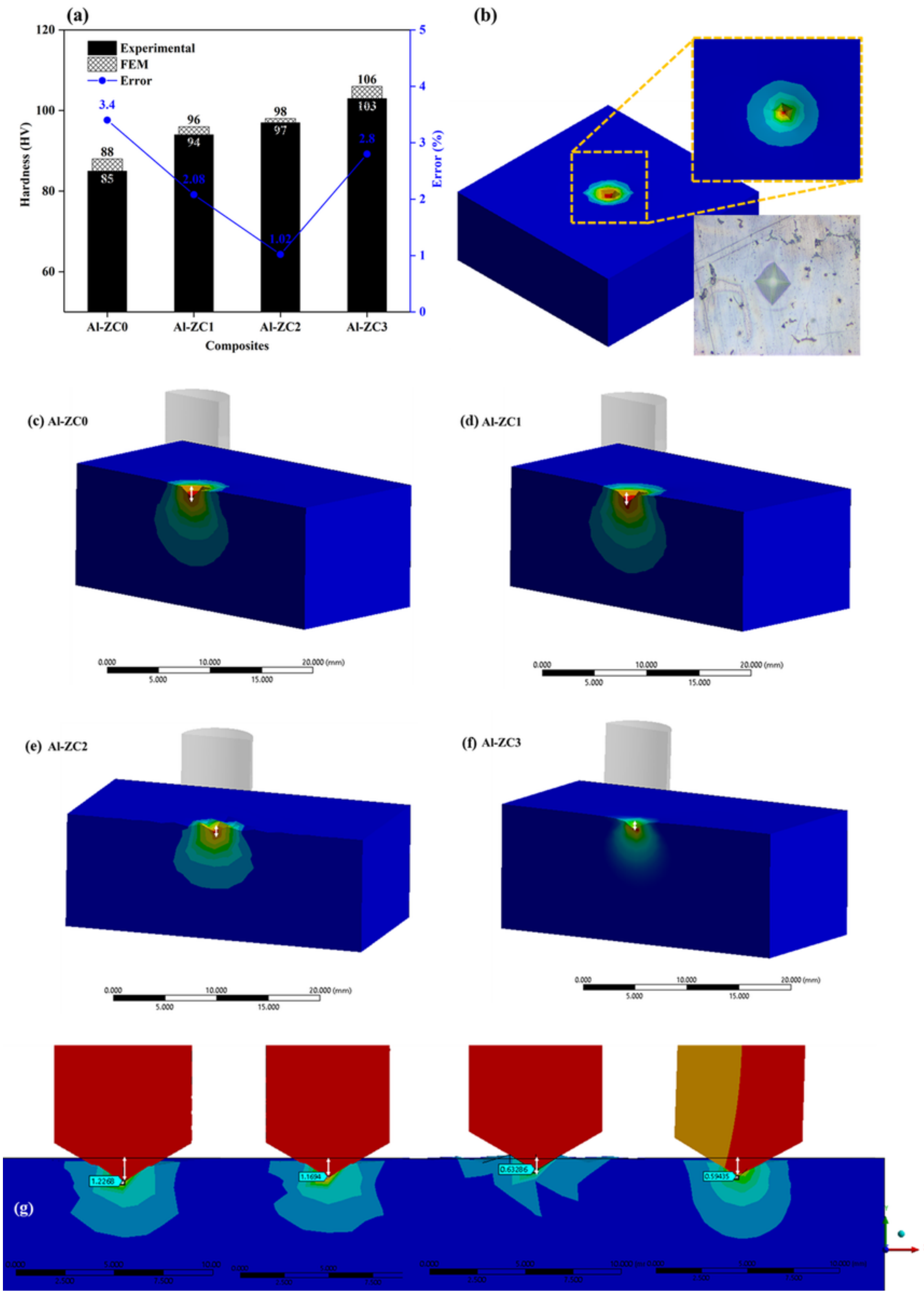

Figure 6

(a) Variation of experimental and FEM hardness along with error (%) of the composites, (b) Experimental indentation versus FEM and (c - f) Finite element simulation for indented profile of composite specimen (c) Al-ZC0, (d) Al-ZC1, (e) Al-ZC2, (f) Al-ZC3 and their respective (g) indentation depth

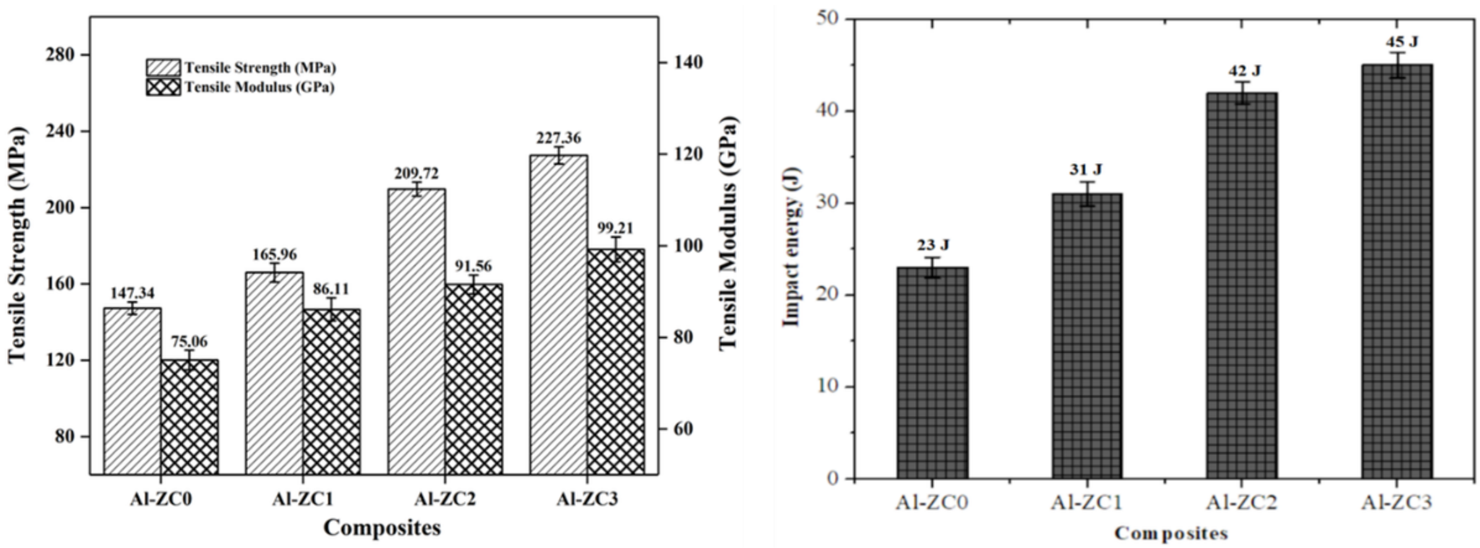

Figure 7

(a) Tensile strength and tensile modulus of fabricated composites and (b) Impact energy of the composites

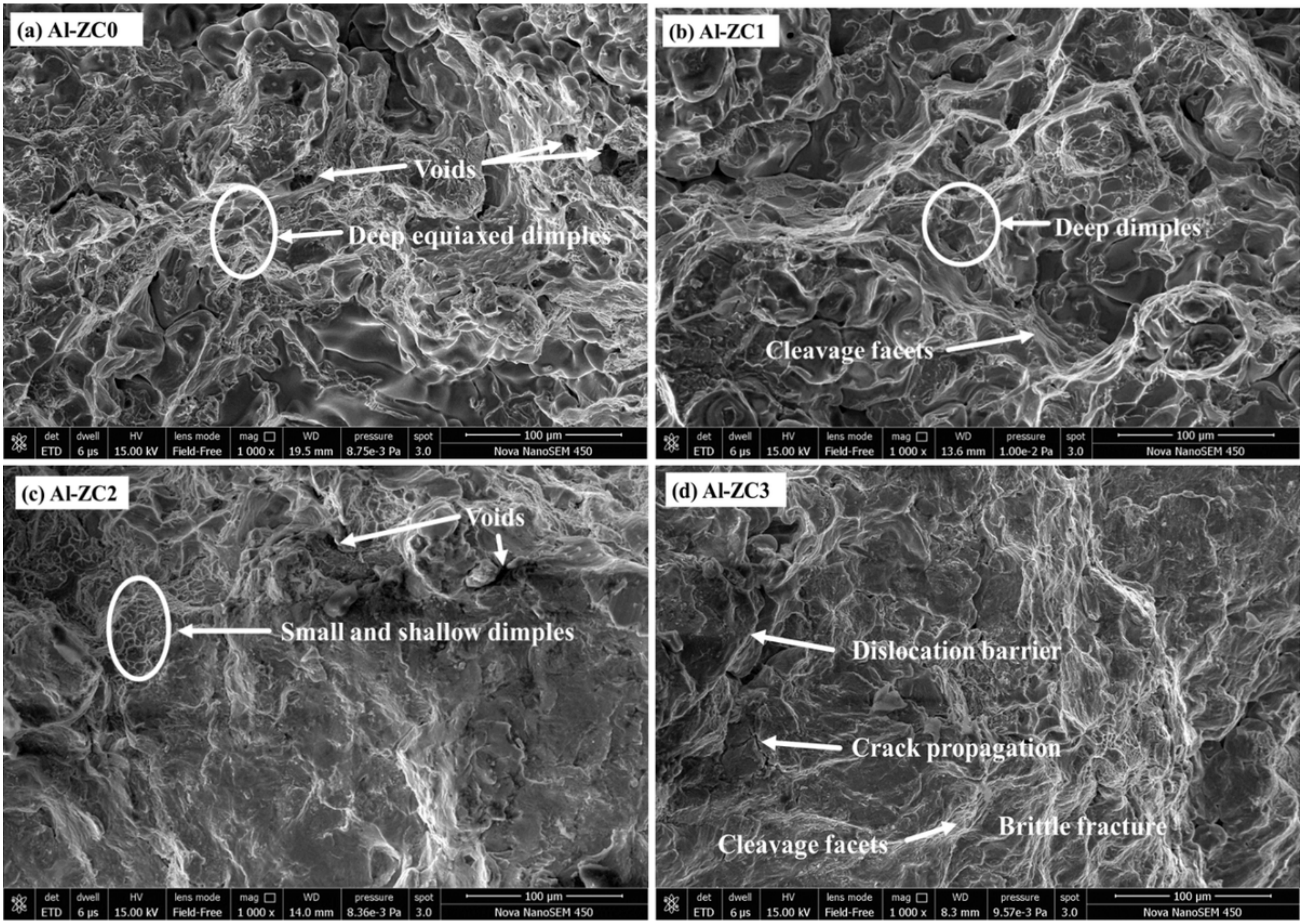

Figure 8

Fractured surface morphology (a) Al-ZC0, (b) Al-ZC1, (c) Al-ZC2 and (d) Al-ZC3

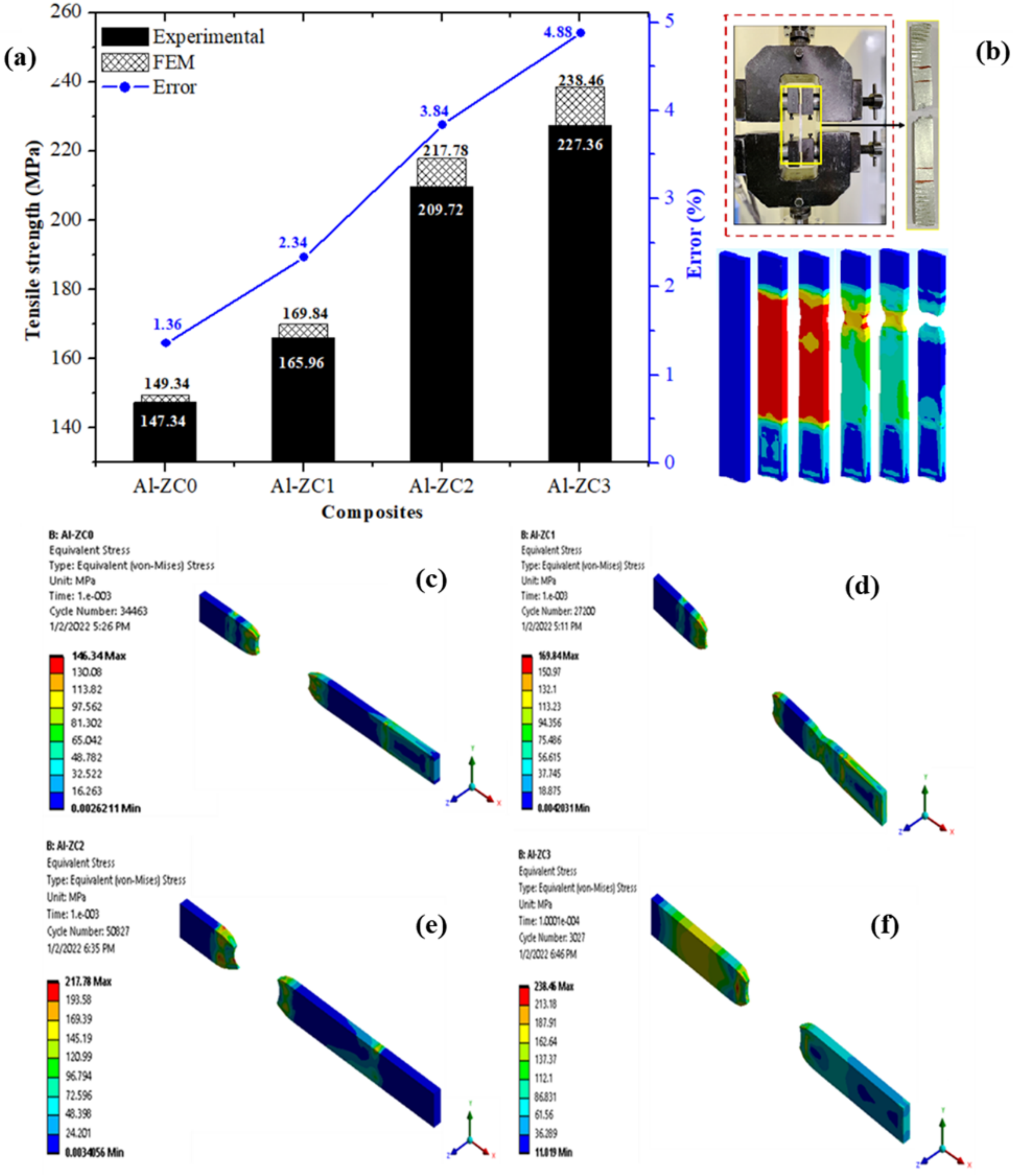

Figure 9

Variation of (a,b) experimental and FEM tensile strength along with error (%) of the composites and FEM simulation contour plots of tensile strength for (c) Al-ZC0, (d) Al-ZC1, (e) Al-ZC2, and (f) Al-ZC3

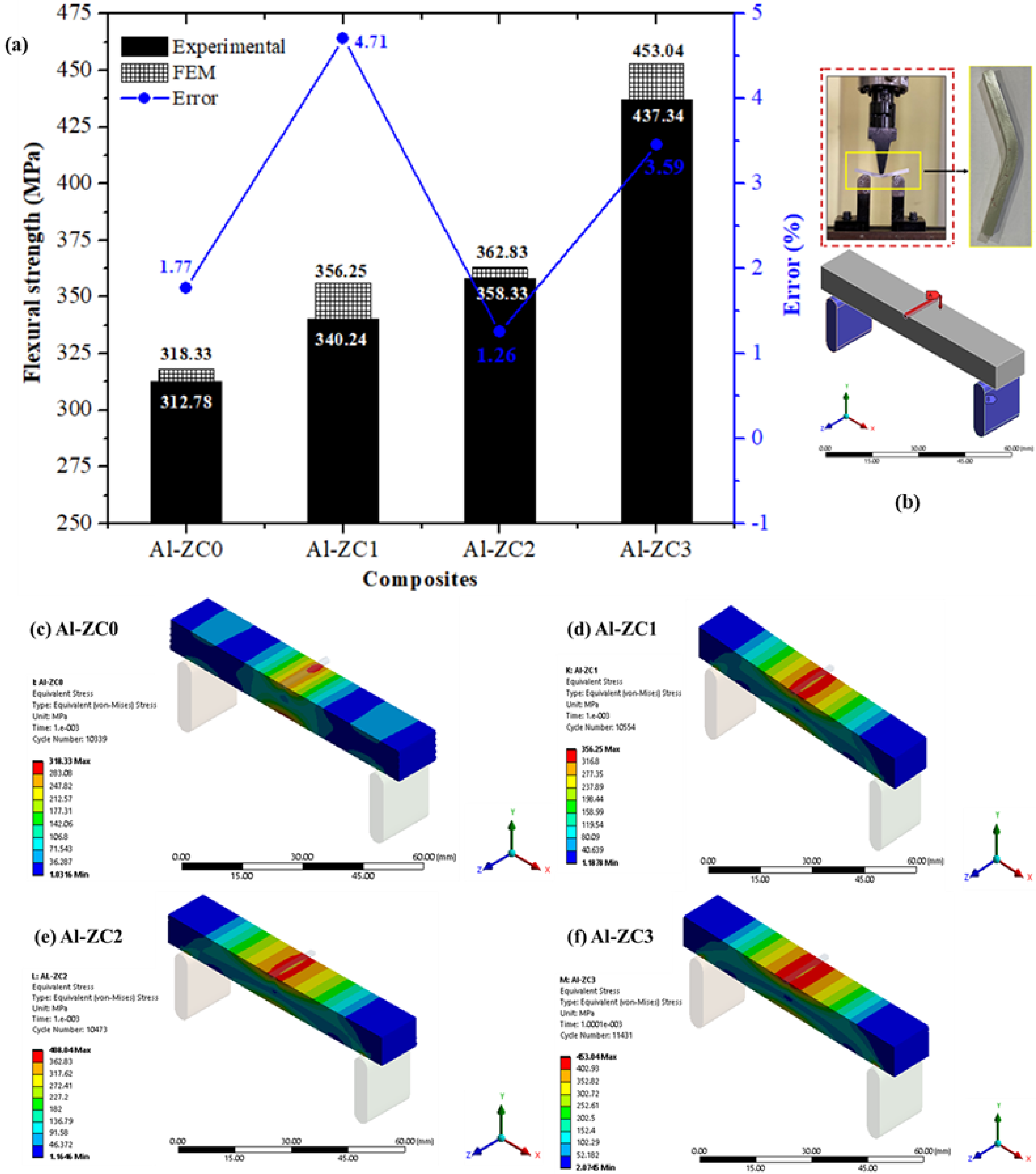

Figure 10

Variation of (a,b) experimental and FEM flexural strength along with error (%) of the composite sand contour plot for flexural test (c) Al-ZC0, (d) Al-ZC1, (e) Al-ZC2, and (f) Al-ZC3

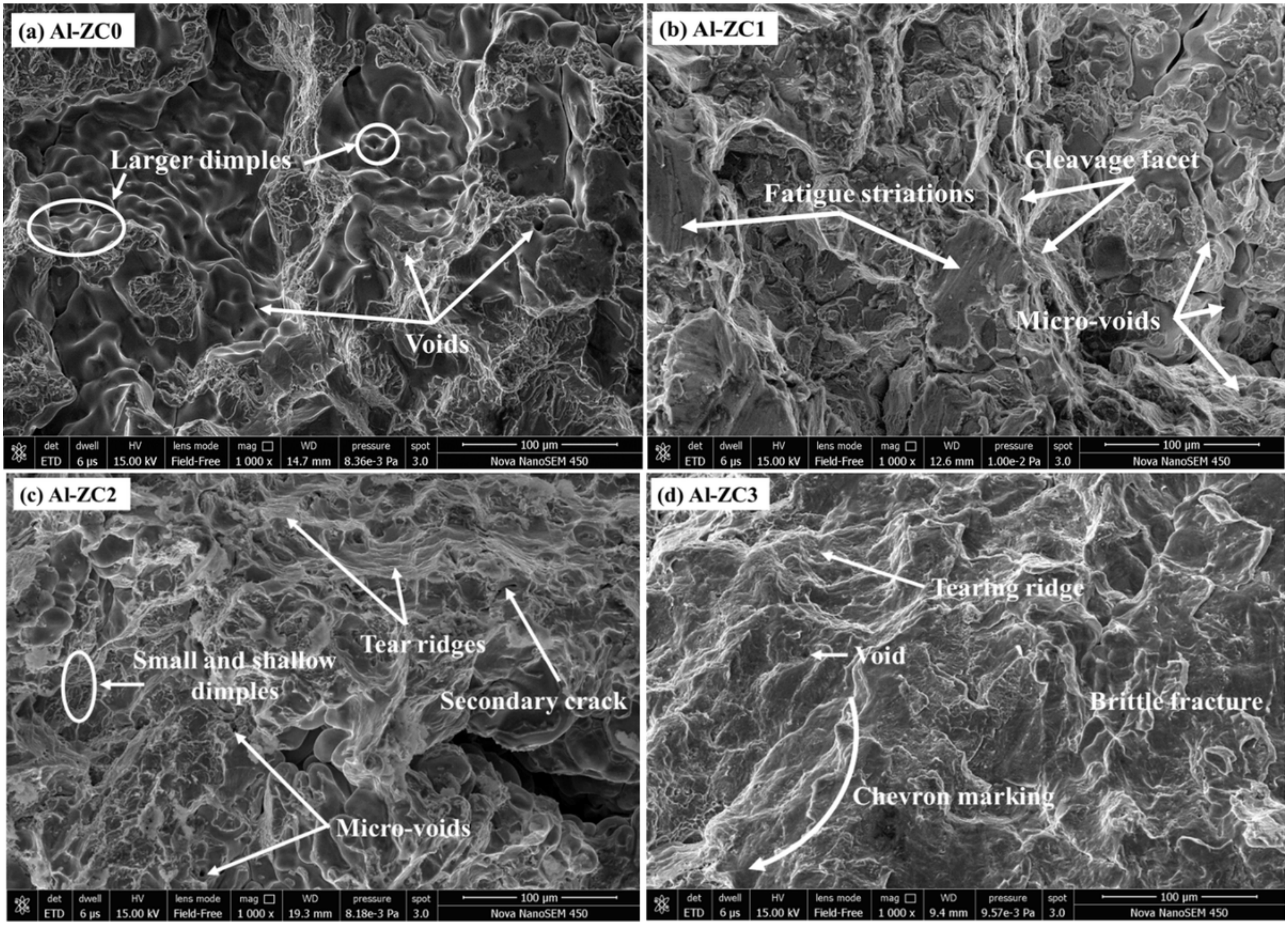

Figure 11

SEM micrographs of the impact fractured samples of (a) Al-ZC0, (b) Al-ZC1, (c) Al-ZC2, and (d) Al-ZC3